LA-UR- 97-2498

Title: MULTI-GROUP FOKKER-PLANCK PROTON TRANSPORT IN MCNP

CONF-971125--

Author(s): K. J. Adams

Submitted to: Embedded topical meeting at 1997 Winter ANS meeting, Albuquerque, NM, November 16-20, 1997

Los Alamos
NATIONAL LABORATORY

Form No. 836 R5
ST 2629 10/91

DISCLAIMER

Multi-group Fokker-Planck Proton Transport in MCNP™*

Kenneth J. Adams
Los Alamos National Laboratory
Los Alamos, NM

Abstract

MCNP[1] has been enhanced to perform proton transport using a multigroup Fokker-Planck (MGFP) algorithm with primary emphasis on proton radiography simulations. The new method solves the Fokker Planck approximation to the Boltzmann transport equation for the small angle multiple scattering portion of proton transport. Energy loss is accounted for by applying a group averaged stopping power over each transport step. Large angle scatter and non-inelastic events are treated as extinction. Comparisons with the more rigorous LAHET*[2] code show agreement to a few per cent for the total transmitted currents. The angular distributions through copper and low Z compounds show good agreement between LAHET and MGFP with the MGFP method being slightly less forward peaked and without the large angle tails apparent in the LAHET simulation. Suitability of this method for proton radiography simulations is shown for a simple problem of a hole in a copper slab. LAHET and MGFP calculations of position, angle and energy through more complex objects are presented.

Introduction

At several recent experiments at Los Alamos Neutron Science Center (LANSCE) and the AGS at BNL, the viability of high energy proton accelerators for use as radiographic probes has been demonstrated. The high energy proton beam is incident on a target and will undergo attenuation through nuclear collisions. As a result of these interactions the beam will be attenuated by the material in the target. On a detector down stream an image of the target can be obtained where bright spots (high proton intensity) would represent regions of less material and dark areas, were the proton intensity is less, would represent more material. However, the protons also under Coulombic interactions as they pass through the target. These interactions cause energy loss and small angle deflections. The deflections would cause a blurring of the image and hence reduce the resolution of the image. The effect of the multiple scattering can be compensated for by magnetic lensing systems but the lenses are tuned for certain energy protons which requires a good understanding of the energy losses the protons will have. Thus accurate simulation tools are needed to support the experiment design, and analysis and interpretation of the data. Further, the ability to generate a radiograph of the object to be radiograhped is an invaluable predictive tool to assess the accuracy of the predictive model.

The LAHET code system provides the best high energy proton beam simulation available but it suffers from certain limitations in the geometries it can describe and the computer systems on which it can run. MCNPX[3] will have fewer of these limitations while having all the needed physics models but is in the development phase. However, MCNP is available today and has the capability with the adaptions presented below to transport high energy protons using its multi-group Fokker Planck (MCFP) algorithm.

---

*. MCNP and LAHET are trademarks of the Regents of the University of California, Los Alamos National Laboratory

This paper will first present an overview of the motivation of the use of the Fokker-Planck (FP) equation for describing charged particle transport as a foundation for method. Since the derivation of the FP equation has been presented elsewhere, we will only present the features needed to describe the Fokker-Planck algorithm in MCNP that is used to transport protons. Next, the particular adaptions to this scheme which make it a useful tool for proton radiography calculations will be discussed. The model is adequate to account for the small angle scattering that the protons undergo in the target without giving non-physical ray artifacts. The method for choosing the parameters of the scattering model will discussed. Then comparisons with LAHET for 800 MeV protons on slabs of material will be presented. We will also compare the Monte Carlo simulation and a deterministic method of solution. The good agreement between the two modes of solving the same provides a bridge for future higher dimensional deterministic simulations. The one dimensional simulations show that the method has satisfactory accuracy for the regions of proton phase space relevant to proton radiography and suitable generality to model arbitrary material configurations. The next section will present comparisons with LAHET for a more complex geometry, representative of a candidate proton radiography target. Finally, we will compare recent data taken at LANSCE and simulations.

Method Description

This section presents an overview of the Monte Carlo solution of the FP equation. We begin by reviewing how the FP equation can be derived from the Boltzmann equation; this helps derive the various parameters we will use in the transport calculation, such as stopping power or momentum transfer. With the continuous energy FP in hand, we will specialize to the multigroup approximation of that equation. Finally, we will outline how MCNP solves this equation.

The time independent Boltzmann equation is

$$\hat{\Omega} \bullet \nabla\varphi + \Sigma_T\varphi - \int \Sigma_S(r;E', \Omega' \rightarrow E, \Omega)\varphi(r;E', \Omega')dE'd\Omega' = Q_{ext}$$

where φ is the angular flux and Σ_T is the total macroscopic cross section (units 1/cm), Σ_S is the scattering cross section and Q_{ext} is the source term. The first approximation[4,5] is to assume that Σ_S can be separated into an elastic scattering term which leaves the energy unchanged but allows for deflections in the direction in which the particle travels, Q_{el}, and an inelastic term which leaves the direction unchanged but accounts for an energy loss, Q_{in}. Then Drumm[5] has shown that a Taylor expansion of the Boltzmann equation leads to the following FP equation where the Q terms are the FP approximation:

$$\hat{\Omega} \bullet \nabla\varphi + \Sigma_T\varphi - Q_{el} - Q_{in} = Q_{ext}$$

The inelastic term is:

$$Q_{in} = \Sigma_{in}(E)\varphi(E, \hat{\Omega}) + \frac{\partial}{\partial E}[S(E)\varphi(E, \hat{\Omega})] + \frac{1}{2}\frac{\partial^2}{\partial E}([\sigma_E(E)\varphi(E, \hat{\Omega})]) + \ldots$$

Σ_{in} is the total inelastic cross [1/cm], S is the stopping power [MeV/cm], which is dE/dx, σ_E is the second moment of the inelastic cross section [MeV^2/cm] which essentially describes energy loss straggling. In this work we have neglected energy loss straggling and will discuss its impact on proton radiography calculations later.

The elastic term can be written as:

$$Q_{el} = \Sigma_{el}(E)\varphi(E,\hat{\Omega}) + \frac{\alpha}{2}\left\{\frac{\partial}{\partial\mu}\left[(1-\mu^2)\frac{\partial}{\partial\mu}\varphi(E,\hat{\Omega})\right] + \frac{1}{(1-\mu^2)}\frac{\partial^2}{\partial\phi^2}\varphi(E,\hat{\Omega})\right\} + \ldots$$

where Σ_{el} is the total elastic cross section [1/cm], α is the momentum transfer [ster/cm], given by:

$$\alpha = 2\pi\int\Sigma_{el}(E,\mu')(1-\mu')d\mu'$$

where $\Sigma_{el}(E,\mu')$ is the differential elastic scattering cross section. Morel[4] has shown that the differential elastic scattering operator (the term in braces) can be satisfactorily be approximated by the following integral operator as μ_{FP}->1:

$$B_\alpha\psi = \int_0^{2\pi}\int_{-1}^{1}\sigma_{FP}(E,\mu_0)\psi(E,\hat{\Omega}')d\hat{\Omega}' - \sigma_{FP}\psi$$

where

$$\sigma_{FP}(E,\mu_0) = \frac{\alpha(E)}{1-\mu_{FP}}\frac{1}{2\pi}\delta(\mu_0-\mu_{FP})$$

and μ_{FP} is the Fokker Planck scattering angle which is a variable. We will discuss ways of choosing μ_{FP} for efficacious calculations.

In this formulation, the total cross section has been replaced by an absorption cross section which is:

$$\Sigma_A = \Sigma_T - \Sigma_{el}(E) - \Sigma_{in}(E)$$

Thus, if the absorption cross section is known or assumed then the total elastic and inelastic are not really needed. Also note, I have neglected the position dependence on all the above as a convenient short hand even though when the transport equation is solved position dependence will be taken into account. By absorption we mean catastrophic and assume that a proton and any subsequent progeny are lost from the beam. Thus we use the "nonelastic" of Janni[6] to represent this removal or absorption cross section at this level of approximation.

For this algorithm to work, there are three physical quantities needed, the stopping power, S, the momentum transfer coefficient, α, and the absorption cross section, Σ_A. For the present

work, these transport quantities were taken from the evaluation of Janni[6,7]. We note that there are several different elastic[8] and nonelastic[9,10] cross section evaluations available and work is proceeding in the APT[11] and proton radiography programs on selecting the best evaluation. Finally, we note that we use Bragg additivity to combine microscopic versions of the above quantities for the transport calculation. This may not be as precise as other prescriptions for the stopping power but introduces only a small per cent error in the final calculation.

Finally this algorithm is multigroup. In generating the transport quantities, we have assumed a flat flux across the energy group and assumed that cross sections are flat enough that the group average is equal to the value at the group midpoint. Then to summarize for MCFP transport there are essentially three interactions which can occur, absorption, angular deflection, and energy loss. For our purposes, absorption is treated as the non-elastic scattering cross section, σ_{NE}, of Janni, the cross section for the angular deflection is $\sigma_{FP}\delta(1-\mu_{FP})/2\pi$, and stopping power is the energy loss cross section. A transport cross section is formed by the sum of the non-elastic and σ_{FP} cross sections. This is used in the usual way to determine a mean free path to an interaction. If this path length is longer than the distance it would take the particle to lose enough energy to change groups, then it undergoes only an energy loss event with no change in direction and goes to the next highest energy group. Otherwise, it can be absorbed or deflected. If it is deflected some of the amount of energy lost is the stopping power times the pathlength. The particle is transported until it escapes, is absorbed, or its energy falls below cutoff.

Particular adaptions for proton radiography

The Fokker-Planck scattering angle is a variable and needs to be chosen with some care if the simulation is to provide a reasonable picture of reality. The transport method described above has been implemented in MCNP with a fixed FP scattering angle whose cosine is 0.9. This value is too large for most proton radiography calculations as shown in Fig. 1 where the exit current is plotted as a function of cosine of exit angle for 110 group 800 MeV protons on 11.2 cm of copper (The protons were started in the first group which means their actual incident mean energy was 819 MeV). The angular distribution showed an anomalous peak at μ=0.9. This was the result of having a very low probability of FP scatterings occurring in the slab of copper. Usually no FP events occurred, infrequently one would occur, and more than one almost never. Hence the peak in the distribution at μ=0.9. Moreover, Fig. 2 shows the exiting energy spectrum which has an anomalously large tail due to the infrequent increased trajectories.

To investigate the effect of the value μ_{FP} several runs were done with the scattering angle fixed to smaller and smaller values (cosines progressively closer to unity.) The results for μ_{FP}= 0.9, 0.99, 0.999, 0.9999, 0.99999 are shown in Figs. 3 and 4. Fig. 3 shows the range of cosine theta from 0.5 to 1 and Fig. 4 shows the range from 0.9 to 1. The curves with μ_{FP} less than 0.999 show an anomalous scattering peak near μ_{FP}. With μ_{FP} on the order of 0.9999 and larger, the results seem converged. This can be understood in terms of the process by which the momentum transfer is related to a "scattering cross section." According to Morel, et. al., in ref. 4

$$\sigma_{FP} = \frac{\alpha}{(1-\mu_{FP})}$$

For 800 MeV protons, α is on the order of 1e-4 ster/cm in copper (cf. Table 10 of ref. 3). Thus to have any appreciable probability of FP scattering in 11.2 cm of copper, μ_{FP} needs to be larger than 0.999.

However, using a fixed μ_{FP} is not a very general solution nor necessarily very efficient. Following the condensed history approach used for electrons (ref. 8), the probability of FP scatter should be approximately the probability for undergoing an energy loss event in the "energy" step or group. In electron transport, angular deflections occur in an energy substep, so in fact an electron will undergo several deflections before going to another "energy group." Thus if we desire to have the probability of energy loss event with no deflection approximately equal to deflection and absorption then this leads to a natural selection for μ_{FP}.

$$\frac{S_g}{\Delta E_g} \cong \sigma_{NE,\,g} + \frac{\alpha_g}{(1-\mu_{FP}(g))}$$

where the g subscript refers to energy group, S_g is the stopping power averaged over the group, $\sigma_{NE,g}$ is the non-elastic multigroup cross section, α_g is the multigroup momentum transfer, ΔE_g is the energy group width. Then the FP scattering angle can be written as a function of group as:

$$\mu_{FP}(g) = 1 - \frac{\alpha_g}{\left[\frac{S_g}{\Delta E_g} - \sigma_{NE,\,g}\right]}$$

This solution is applicable for all cases where the group structure (energy grid) is fine enough for the problem geometry. It may lead to many small FP events for "thick" problems but for proton radiography purposes it should be adequate. There may be other choices for μ_{FP} which we have not explored

Figs. 3 and 4 also include a comparison of the exit current angular distributions calculated with $\mu_{FP}(g)$ and the ONEBFP deterministic code[12,13] with the fixed μ_{FP} results already discussed. The agreement is quite good for all converged μ_{FP} results where by converged it is meant that $\mu_{FP} \geq 0.9999$. The ONEBFP deteministic code which solves the 1D differential version of eq. (2) with all the same cross sections and approximations, seems to be slightly less forward peaked than MCFP and have a slightly higher tail. Part of these discrepancies may be attributed to the fact that MCFP was run for a mono-energetic source whereas the deterministic code used a Gaussian. Table 1 summarizes some of the integral quantities calculated by both codes. Also the table shows the relative timing for the various MCFP problems. The exiting energy spectrum is presented in Fig.

5 for the various calculations. The spectra have the intuitively correct mean value ~650 MeV (For the group structure, 110 2 MeV wide bins with highest midpoint at 819 MeV, so an incident proton in the first group has a mean energy of 819 MeV.) The high loss tails for the large FP angles (μ_{FP} further from unity) reflect the result of the anomalous scattering and hence longer pathlengths. The deterministic result is not presented since it had negative components, though the correct mean for the Gaussian problem.

Table 1: Comparison of exit currents for 800 MeV protons on 11.2 cm of Copper

Code/method	Exiting Current (F1 tally)	Particles per minute
ONEBFP/deterministic	0.487	
MCNP/MCFP default	9.99910E-01 .0000	1.7950E+04
MCNP/MCFP μ_{FP}=0.9 +att.	4.86097E-01 .0010	2.3842E+04
MCNP/MCFP μ_{FP}=0.99	4.85967E-01 .0010	2.3761E+04
MCNP/MCFP μ_{FP}=0.999	4.86463E-01 .0010	2.2723E+04
MCNP/MCFP μ_{FP}=0.9999	4.86394E-01 .0010	1.5839E+04
MCNP/MCFP μ_{FP}=0.99999	4.86638E-01 .0016	3.9316E+03
MCNP/MCFP μ_{FP}(g)	4.88690E-01 .0032	1.1226E+04

Similar results were obtained for the 10 GeV case as shown in Fig. 5 for the exiting angular current. Once again the agreement between the two methods, deterministic and Monte Carlo, is very good. The integral quantities are in equally good agreement.

To determine if this method works for an arbitrary material several comparisons were made with LAHET for 800 MeV protons incident on a slab of high explosive[14]. Recall that one of our major approximations is that the stopping powers can be added together microscopically and here is where we test that approximation. Figure 6 shows the angular distribution of the exit current for angles from 30 milliradians to zero. The final bin is over the range of 10 mr, the range of greatest interest for proton radiography at LANSCE, where the codes are in 3% agreement. For larger angle scatter the agreement is not as good though still quite reasonable as can be seen in Figure 7. Included in Figure 7 is a TRIM[15] simulation which is more of a single event Monte Carlo calculation. Using this as a context for the level of agreement, LAHET and MCFP calculations are quite good. Moreover, the trends of the distributions are quite consistent with the theoretical speculations of Borghers[19]. Finally, Table 2 lists the total transmitted currents calculated with LAHET and MCFP.

The agreement is to within a few per cent.

Table 2: Comparison of Net Exiting Current for 819 MeV Protons on 11.2 cm of HE

Density	LAHET	MCFP
1	8.72156E-01 0.0004	8.86570E-01 .0011
1.9	7.68240E-01 0.0005	7.97210E-01 .0016
2.5	7.04749E-01 0.0006	7.41640E-01 .0019

3D simulations

One of the main reasons to have a Monte Carlo technique like the Fokker-Planck transport of protons is to be able to transport particles in a complex three dimensional object without sacrificing geometrical fidelity. The one dimensional examples above could be done much more efficiently with deterministic codes (ref. 12,13) but for more exotic geometries further approximations are still needed for the deterministic codes in regards to both the method and geometrical representation. Moreover, the Monte Carlo simulation can provide a detailed phase space description of the exiting current to be used in appropriate lensing or magnetic tracking codes.

As an initial problem, the copper slab simulation above was run with a 1 cm diameter hole in the interior. The proton flux was scored on a lattice detector grid one meter from the target. The beam was a flat disk with uniform energy of 800 MeV. Figure 9 shows a line-out across the detector plane. The solid curve is the simulation with the hole and the dashed without. Clearly, the hole is present and the edges can be estimated from the figure.

A more stressing simulation geometry is presented in Figure 10[16]. The figure presents the density profile in high explosive 2.5 μsec after detonation. The geometry was modeled as a set of concentric spheres for the LAHET[17] and MCFP simulations. Figure 11 shows the comparison of MCFP and LAHET for various angle cuts[17]. The effect of the angle cuts is too remove protons from the beam which have exit angles greater than the cut values and is effectively an ideal lensing collimator. At 20 mr, MCFP is tending to predict more scattering than LAHET. For 10 mr, the nominal lens setting for the experiment, the agreement between the codes is quite good and is equally good at 5 mr. Figure 12 shows the energy spectrum[17]. Once again for the magnets tuned to the nominal value, the agreement between LAHET and MCFP is quite good.

Finally, we compare our best simulation for the onion skin experiment. Figure 13 shows the calculated radiograph at 2.5 μsec where the high explosive was modeled with spherical symmetry. Figure 14 is preliminary data taken at LANSCE[18]. Quantitative features are beyond the scope of this paper, but the agreement in dynamic range and qualitative features is outstanding. Even experimental features, such as the halo surrounding the object are apparent in the simulation.

Conclusions

The use of the Monte Carlo Fokker Planck algorithm for the transport of high energy protons has been shown to provide adequate simulations for use in proton radiography. The algorithm is expected to be quite reasonable at describing the small angle portions of the beam and gives reasonable agreement with other codes and experimental data. The major features of the algorithm that make it suitable for proton radiography calculations are the group and material dependent Fokker-Planck scattering angle, inclusion of removal as absorption, and Bragg additivity of the stopping powers. Future enhancements include modeling the large angle scattering with appropriate scattering cross section, inclusion of energy loss straggling, and possible improvements of the stopping power formulation.

References:

1) Judith F. Briesmeister, Editor, "MCNP[TM*] -- A General Monte Carlo N-Particle Transport Code, Version 4A," Los Alamos National Laboratory report LA--12625--M (November, 1993).
2) R. Prael and H. Lichtenstein, "User Guide to LCS: The LAHET Code System", LA-UR-89-3014 (1989)
3)H. G. Hughes, R. E. Prael, R. C. Little, "MCNPX - The LAHET/MCNP Code Merger," X-Division Research Note, XTM-RN (U) 97-012, April 22, 1997.
4) J. E. Morel, L. J. Lorence, R. P. Kensek, J. A. Halblieb, and D. P. Sloan, "A Hybrid Multigroup/ Continuous-Energy Monte Carlo Method for Solving the Boltzmann-Fokker-Planck Equation," Nuc. Sci. & Eng. **124**, 369-389 (1996)
5) C. Drumm, W. C. Fan, J. H. Renken, "Forward and Adjoint Methods and Applications for Deterministic Electron-Photon Transport," Nuc Sci. Eng. **108**, 16-49 (1991)
6) J. F. Janni, "Proton Range-Energy Tables, 1 keV - 10GeV", Atomic Data and Nuclear Data Tables, **27**, 2/3, (1982)
7) code provided by N. King of P-25 at Los Alamos National Laboratory
8) M.J. Berger, Monte Carlo calculation of the penetration and diffusion of fast charged particles," Methods in Computational Physics, vol. 1, Academic Press, New York, (1963)
9) W. Bauhoff, "Tables of reaction and total cross sections for proton-nucleus scattering below 1 GeV," Atomic Data and Nuclear Data Tables, 35, 429-447 (1986)
10) R. F. Carlson, "Proton-Nucleus total reaction cross sections and total cross sections up to 1 GeV," Atomic Data and Nuclear Data Tables, 63, 93-116 (1996)
11) R. E. Prael and M. B. Chadwick, "Applications of Evaluated Nuclear Data in the LAHET code," presented at the International Conference on Nuclear Data for Science and Technology, May 1997, Trieste, Italy
12) D. R. Marr, R. E. Prael, and K. J. Adams, "Evaluating the ONEBFP code for Possible Use in the Proton Radiography Program," October, 1996
13) D. R. Marr, R. E. Prael, R. E. Alcouffe and K. J. Adams, "Deterministic Proton Transport Solving a One Dimensional Fokker-Planck Equation," presented ANS Winter Meeting, Albuquerque, NM, November 16-20, 1997
14) LAHET calculations provided by R. E. Prael
15) J. F. Ziegler, SRIM: The Stopping and Range of Ions in Matter, IBM Research Instruction Manual (1996)
16) Private communication from J. Sarracino.
17) LAHET calculations provided by K. Morley
18) Private communication from J. Zumbro and K. Morley
19) C. Borgers and E. W. Larsen, "On the accuracy of the Fokker-Planck and Fermi pencil beam equations for charged particle transport," Med. Phys. 23 (10), October, 1996

*. MCNP is a trademark of the Regents of the University of California, Los Alamos National Laboratory.

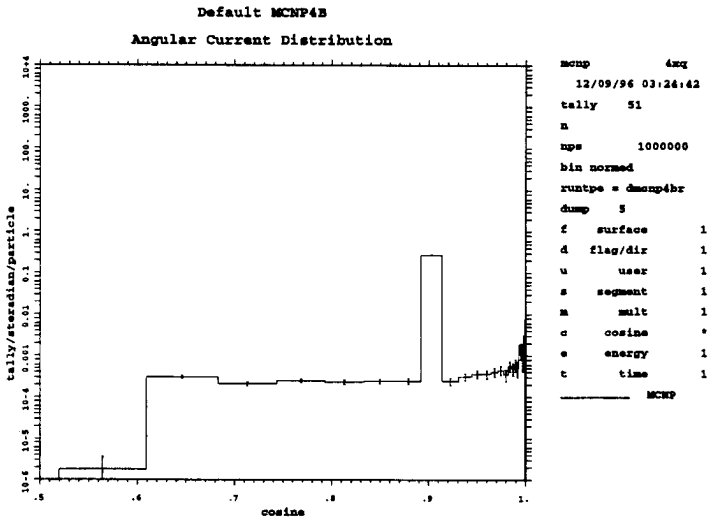

Figure 1: Exiting current angular distribution from 819 MeV protons on 11.2 cm of Copper calculated using default Fokker-Planck transport in MCNP. The total exiting current is 0.9999 and the average energy of the exiting protons is 651 MeV. The average pathlength is 11.2219 cm. The pronounced peak in the distribution at cosine =0.9 is due to the hardwired scattering angle in MCNP.

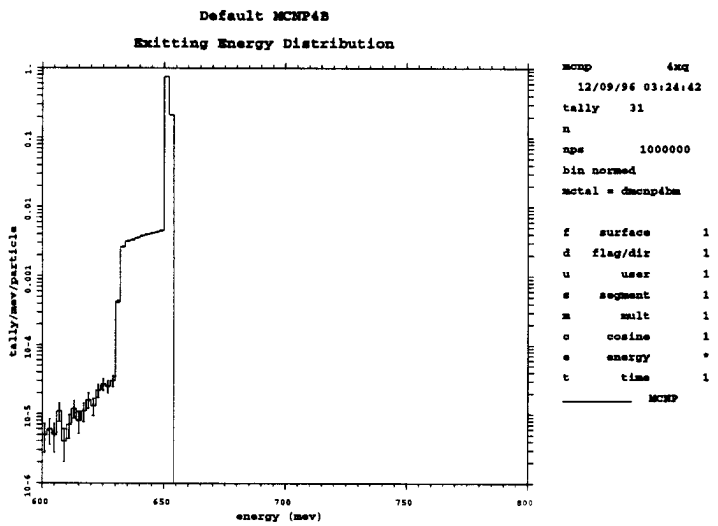

Figure 2: Exiting current energy distribution from 819 MeV protons on 11.2 cm of Copper calculated using default Fokker-Planck transport in MCNP. The distribution shows an anomalously large number of larger than average energy loss events due to the large Fokker-Planck scattering.

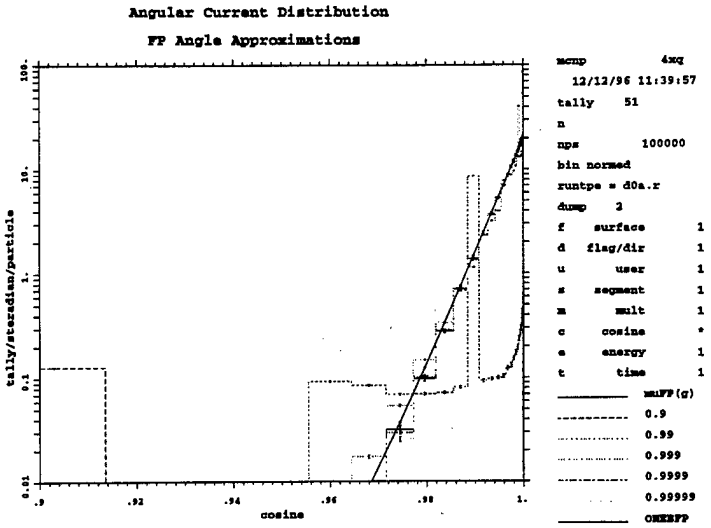

Figure 3 Exiting current angular distribution from 819 MeV protons on 11.2 cm of Copper calculated as a function of cosine of the Fokker-Planck scattering angle using fixed cosines and the group dependent cosine, $\mu_{FP}(g)$. Results from the ONEBFP code are also presented. Anomalous scattering peaks are present near the μ_{FP} when the problem has not converged in scattering angle.

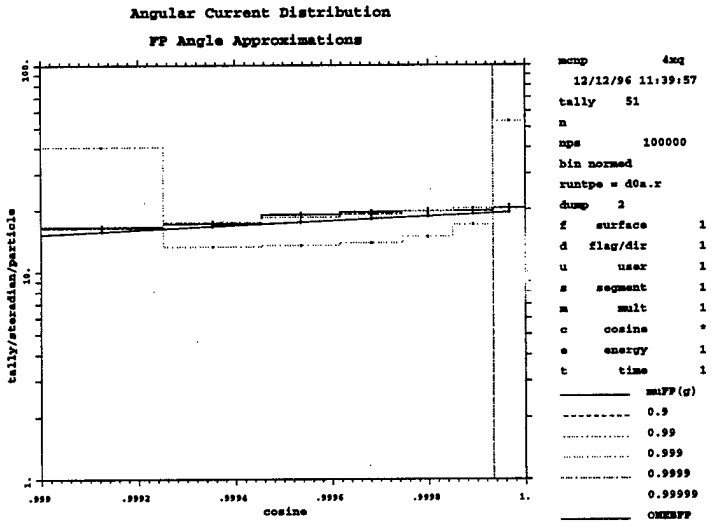

Figure 4: In the angular range of 0 to 45mr the converged fixed scattering angle, $\mu_{FP}(g)$, and deterministic methods are all in excellent agreement. This is the angular range of greatest interest to proton radiography.

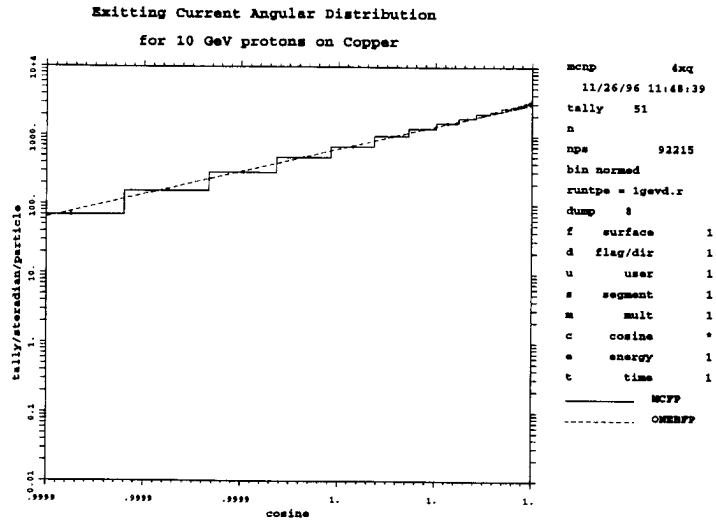

Figure 5: Exiting angular distribution for 10 GeV protons on 11.2 cm of Copper. Comparison of ONEBFP results and MCFP using the group dependent scattering angle cosine. The agreement with ONEBFP is within error bars.

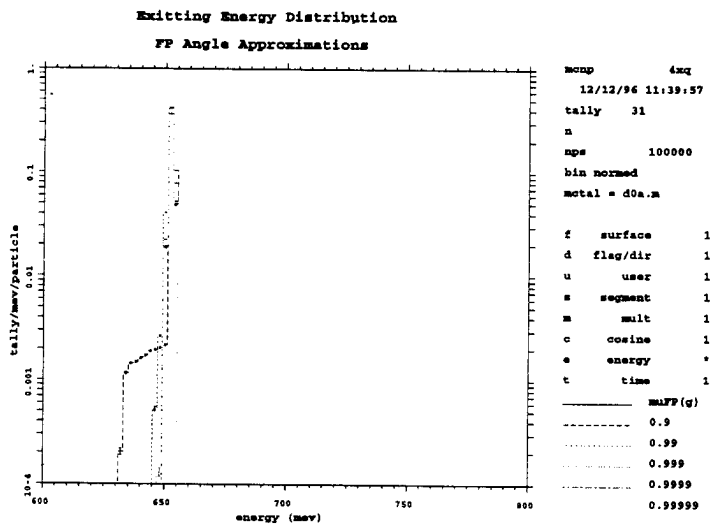

Figure 6: Exiting energy distribution for 819 MeV protons on 11.2 cm of Copper as a function of Fokker-Planck scattering angle. For larger scattering angle, the distribution shows a large energy loss tail due to the artificially large pathlength. Note the energy distribution has width only due to variations in pathlength and not to energy loss straggling which has not yet been included in the model.

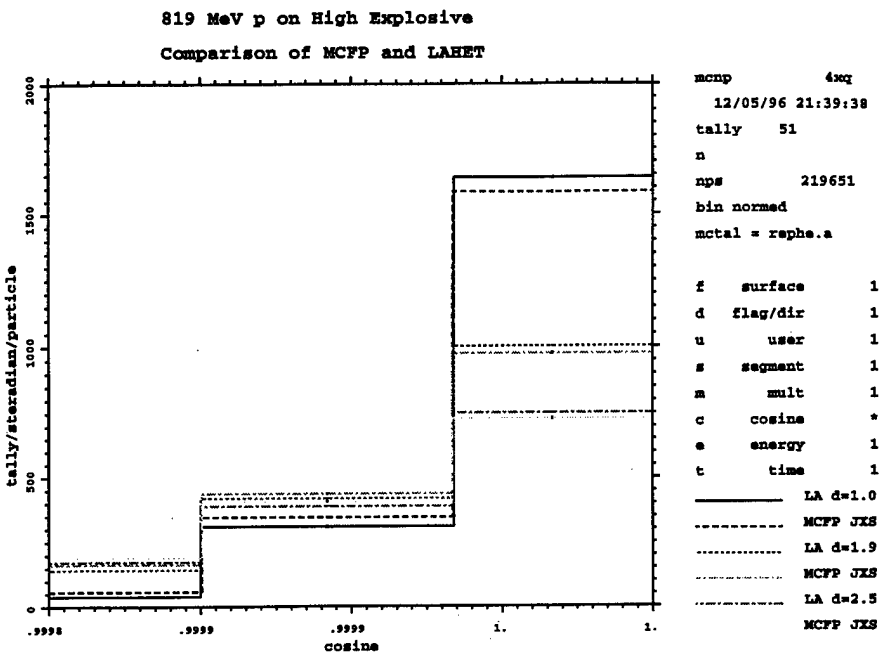

Figure 7: Comparison of LAHET and MCFP calculated exiting current angular distribution for 819 MeV protons of a 10 cm slab of high explosive at three densities (1, 1.9, 2.5 g/cm^3) over the angular range of relevance for proton radiography. The final bin spans 10 milliradians where MCFP and LAHET are within 3% agreement.

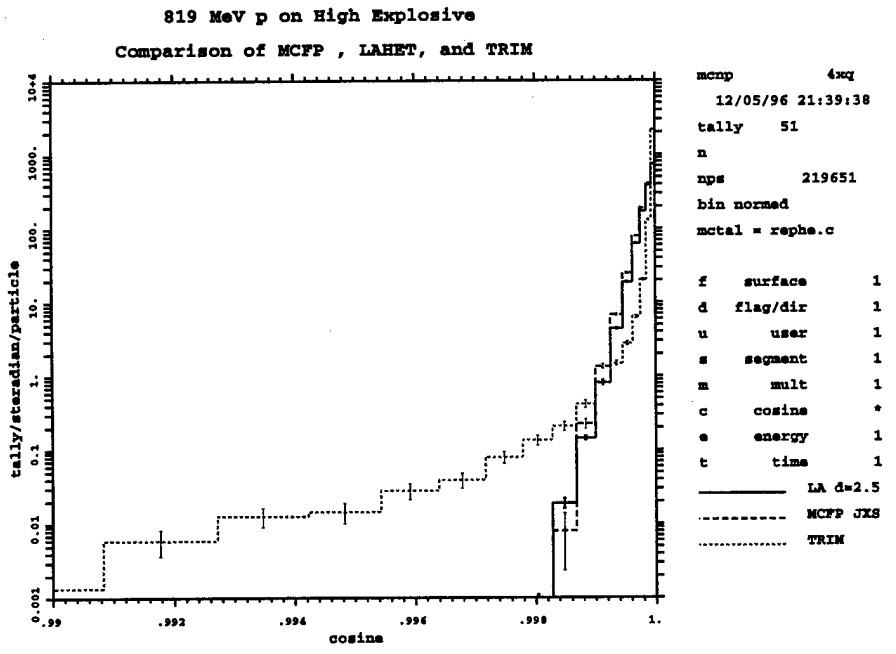

Figure 8: Same comparison as Fig. 7 except the TRIM calculation is included. TRIM is a single event code and hence has a much sharper forward peak and longer large angle scattering tail.

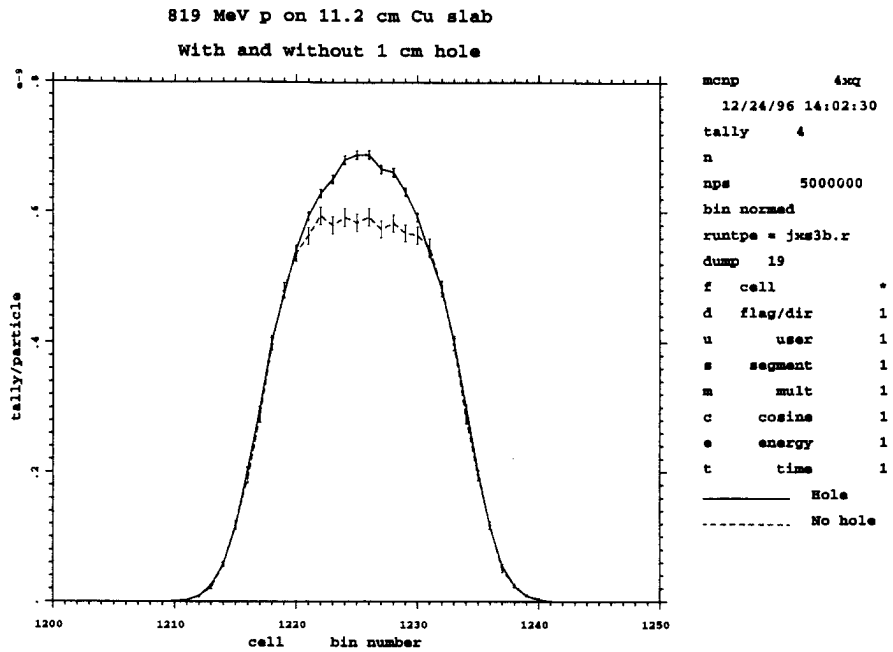

Figure 9: Line out through a lattice flux detector tally near the center of the object with and without a hole in the middle. The differences in tallies (intensities) show marked differences with and without the hole.

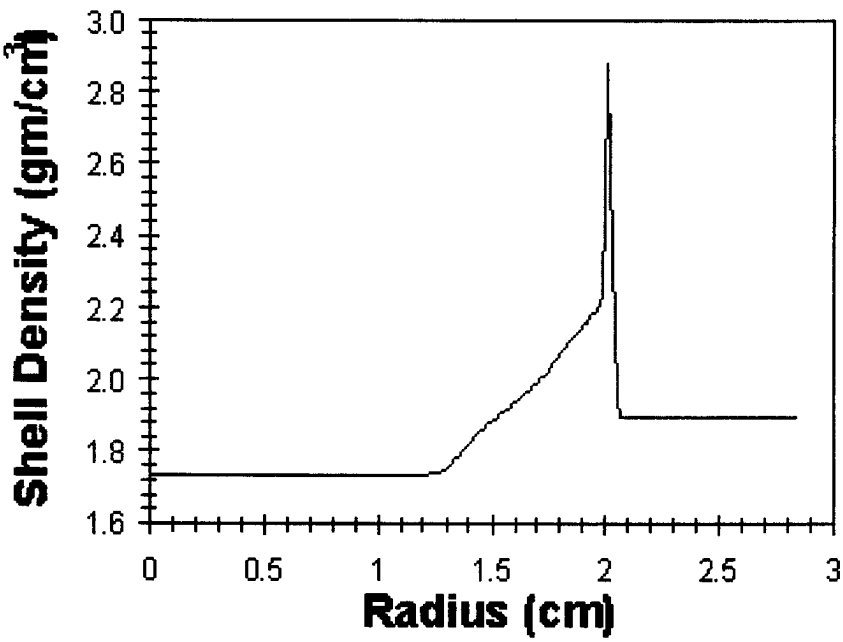

Figure 10: Density profile through the onion skin experiment at 2.5 μsec after detonation. The significant density variations are due to the shock moving out of the object.

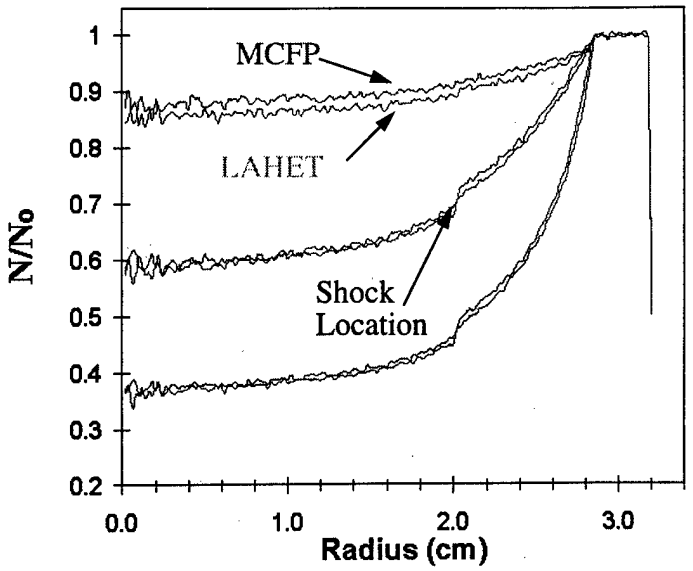

Figure 11: Comparison of transmitted intensities through the spherical object described in Fig. 10 calculated with LAHET and MCFP. The intensities are averaged about an axis of symmetry of the onion skin.

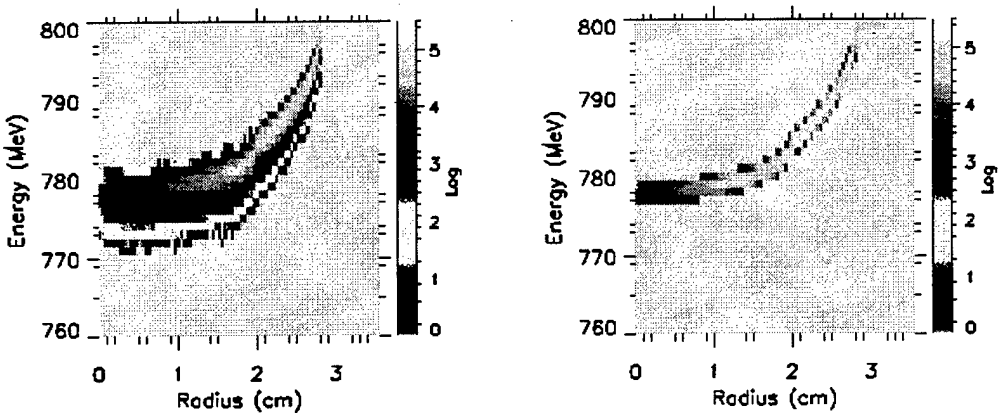

Figure 12: Comparison of calculated energy spectrum through the spherical object described in Fig. 10. The LAHET calculation shows a significant spread due to energy loss straggling but with an intensity about a factor of 100 less than the main CSDA contribution which MCFP calculates.

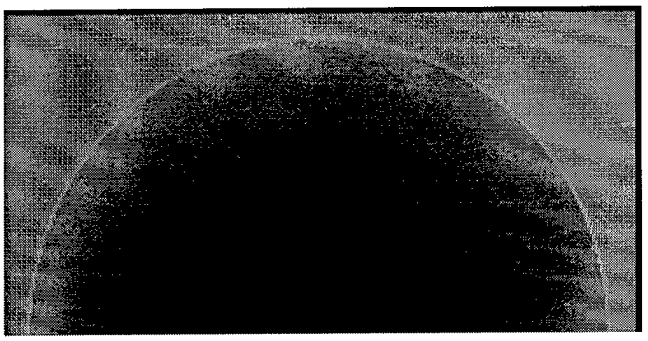

Figure 13: Calculated synthetic radiograph for the onion skin experiment.

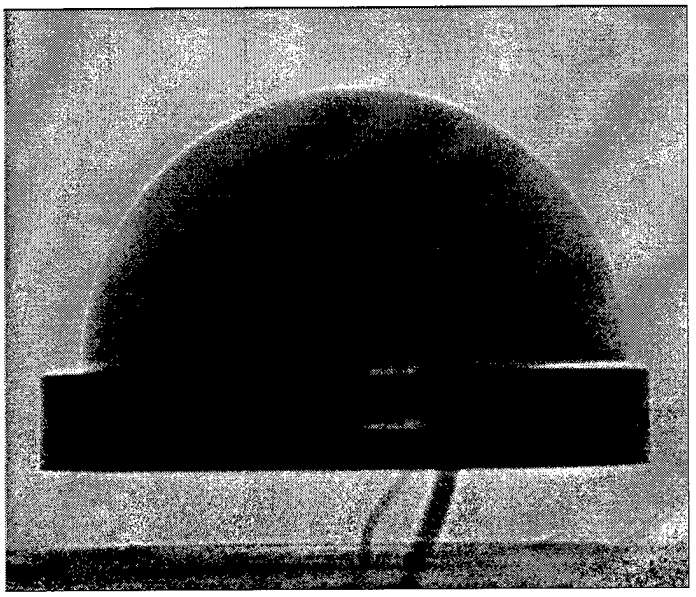

Figure 14: Prelimnary radiograph from the LANSCE experiment on the onion skin.

Report Number (14) LA-UR--97-2497
CONF-971125--

Publ. Date (11) 199708
Sponsor Code (18) DOE/MA, XF
UC Category (19) UC-910, DOE/ER

DOE